Journal of Applied Fluid Mechanics, Vol. 12, No. 1, pp. 77-84, 2019.
Available online at www.jafmonline.net, ISSN 1735-3572, EISSN 1735-3645.
DOI: 10.29252/jafm.75.253.28416

Numerical Simulation of Diffuser of a Gas Turbine using the Actuator Disc Model

S. Sadasivan[1], S. K. Arumugam[2†] and M. C. Aggarwal[3]

[1]*School of Mechanical Engineering, Vellore Institute of Technology, India-632 014*
[2]*CO_2 Research and Green Technologies Centre, Vellore Institute of Technology, India-632 014*
[3]*Department of Mechanical Engineering, Gannon University, PA, USA*

†*Corresponding Author Email: asenthilkumar@vit.ac.in*

(Received September 16, 2017; accepted July 24, 2018)

ABSTRACT

An analysis of the exhaust diffuser section of a gas turbine is presented by incorporating the reduced order mathematical model "actuator disc concept" that represents the last stage of the turbine. The actuator disc model is one of the simplified numerical methods for analyzing the aerodynamic performance of axial turbine stage. In which, the rotor and the stator of the turbine stages are modeled as zero thickness discs with a specified blade speed and zero speed respectively. Finite volume based commercial CFD package ANSYS FLUENT was employed for the numerical investigation of the applicability of the proposed simplified model. The compressible Navier-Stoke equations along with k-ε turbulent model were solved in the computational domain by incorporating suitable boundary conditions. The implementation of actuator disc boundary conditions is described in detail. The numerical results obtained from the proposed model are in good agreement with the experimental data available in the literature. The effect of casing angle on the performance of diffuser is presented.

Keywords: Actuator disc model; Gas turbine diffuser; Flow separation.

NOMENCLATURE

C_f	skin friction coefficient
C_p	pressure coefficient
h	specific enthalpy
H	total enthalpy
$\dot{m}$	mass flow rate
M	Mach number
P	static gas pressure
P_0	total gas pressure
q	heat flux
Re	Reynolds Number
t	time
T	temperature
U	conservative variable vector
u_r	velocity in r-direction
u_z	velocity in z-direction
ψ	loading co-efficient
φ	flow coefficient
ρ	density

1. INTRODUCTION

Diffusers play an important role in the operation of turbomachines by increasing the fluid pressure at the expense of kinetic energy of the fluid. Annular type diffusers are widely used in axial flow turbines. The diffuser decelerates the flow coming out from the turbine exit by converting the kinetic energy of the flow to pressure energy. This pressure recovery permits the turbine exit pressure to be lower than the atmospheric pressure, thus increasing the turbine work output. Ackert (1967) and Venugopal (2015) have showed that a very small change in pressure recovery can significantly increase the efficiency of the gas turbine power plant. The pressure recovery capacity is strongly influenced by the geometrical parameters of the diffuser and flow behaviour at the exit of turbine stage. Interactions between turbine stage and diffuser cause a great challenge in specifying the boundary conditions at the inlet of the diffuser section For the last five decades, many researchers have proposed different numerical methods that suit for the study of turbine diffuser sections. Fleischer *et al.* (1989) employed complete scale model of a gas

turbine diffuser system to figure out the suitable design of various flow-distributing devices for acceptable quality of exhaust velocity distribution. Most of the numerical study on the turbine exhaust systems has been carried out using sector domain by considering the periodicity of the geometry to reduce the computational demand. The computational calculation of such rotating machinery is done with the help of simplified methods like mixing plane, frozen rotor etc. These simplified methods have their own merits and demerits. The actuator disc model is one of such simplified models, which has advantage in terms of reduced computational cost and improved solution accuracy as proposed by Rankine (1865). The actuator disc model is widely used to investigate the flow behaviour across wind turbines. A comparative study between actuator disc model and full rotor CFD models in Réthoré *et al.* (2008) shows that the actuator disc method is capable of capturing the time averaged effect of the rotor in a realistic manner, while maintaining a computational effort two orders of magnitude lower compared with a full physical representation of the rotor. The pressure discontinuity at the infinitely thin permeable disc could produce the same thrust as that of rotating body with finite blades, suggested by Froude (1889). Liu and Hynes (2002) have developed an extension of the actuator disk model to represent the turbine blade rows with highly flared annuli to simulate the asymmetric flows in the coupled domain of turbine last stage and exhaust hood. However, no literature is available on the use of the actuator disk model in a gas turbine diffuser modeling. Hence the present investigation intends to find the suitability of actuator disc model in the analysis of diffuser section attached to the last stage of gas turbine. Also, the paper focuses on the exploration of the effect of the diffuser angle on the performance of the diffuser.

2. COMPUTATIONAL MODEL

The commercial Package ANSYS FLUENT used for the present work solves compressible flow momentum, continuity and energy equations. The compressible Navier-Stokes equations and the $k-\varepsilon$ turbulence model are written in cylindrical coordinate are expressed in vector form as,

$$\frac{\partial(Q)}{\partial t}+\frac{\partial(E)}{\partial r}+\frac{\partial(F)}{\partial z}+H=0 \tag{1}$$

where the vectors are given by,

$$Q=r\begin{bmatrix}\bar{\rho}\\ \bar{\rho}\tilde{u}_r\\ \bar{\rho}\tilde{u}_z\\ \bar{\rho}\tilde{E}\\ \bar{\rho}\tilde{K}\\ \bar{\rho}\varepsilon\end{bmatrix}$$

$$E=r\begin{bmatrix}\bar{\rho}\tilde{u}_r\\ \bar{\rho}\tilde{u}_r\tilde{u}_r+\bar{p}-\bar{\tau}_{rr}\\ \bar{\rho}\tilde{u}_z\tilde{u}_r-\bar{\tau}_{zr}\\ \tilde{u}_r\left(\bar{\rho}\tilde{E}+\bar{p}\right)+\bar{q}_r-\tilde{u}_r\bar{\tau}_{rr}-\tilde{u}_r\bar{\tau}_{zr}\\ \bar{\rho}\tilde{u}_r\tilde{K}-\left(\bar{\mu}+\frac{\mu_t}{\sigma_k}\right)\frac{\partial\tilde{K}}{\partial r}\\ \bar{\rho}\tilde{u}_r\varepsilon-\left(\bar{\mu}+\frac{\mu_t}{\sigma_k}\right)\frac{\partial\varepsilon}{\partial r}\end{bmatrix}$$

$$F=r\begin{bmatrix}\bar{\rho}\tilde{u}_z\\ \bar{\rho}\tilde{u}_r\tilde{u}_z+\bar{p}-\bar{\tau}_{rz}\\ \bar{\rho}\tilde{u}_z\tilde{u}_z-\bar{\tau}_{zz}\\ \tilde{u}_z\left(\bar{\rho}\tilde{E}+\bar{p}\right)+\bar{q}_z-\tilde{u}_r\bar{\tau}_{rz}-\tilde{u}_z\bar{\tau}_{zz}\\ \bar{\rho}\tilde{u}_z\tilde{K}-\left(\bar{\mu}+\frac{\mu_t}{\sigma_k}\right)\frac{\partial\tilde{K}}{\partial z}\\ \bar{\rho}\tilde{u}_z\varepsilon-\left(\bar{\mu}+\frac{\mu_t}{\sigma_k}\right)\frac{\partial\varepsilon}{\partial z}\end{bmatrix}$$

$$H=r\begin{bmatrix}0\\ -\bar{p}+\bar{\tau}_{\theta\theta}\\ 0\\ 0\\ r\left(P-\bar{\rho}\varepsilon\right)\\ \frac{r\varepsilon}{\tilde{k}}\left(C_1P-C_2\bar{\rho}\varepsilon\right)\end{bmatrix}$$

In addition to these set of equations the ideal gas equation (2) is also considered to ensure the closeness of the equations. This equation is given by,

$$\bar{p}=\bar{\rho}R\bar{T} \tag{2}$$

The set of equations governing the fluid flow are based on the following assumptions.

The flow is assumed to be compressible.

1. Ideal gas state is opted for fluid.
2. Fluid flow is considered to be fully developed turbulent flow.

3. GEOMETRICAL DETAILS

The geometrical model of the turbine found in Behr (2007) who carried out experimental studies, has been adopted in the present study. The hub and tip radii of the disc used in the model are 330 mm and 400 mm, respectively. The entire length of turbine

diffuser geometry is 810 mm. The complete details of turbine-diffuser model considered in the present study are shown in Fig. 1. The computational analysis for this model is performed by utilizing the axisymmetric nature of the geometry and flow field. Hence, only a two dimensional geometry was constructed as the computational domain, instead of considering whole 3D geometry. The computational domain was meshed with body fitted structured quadrilateral grids using ICEM CFD software. A sample meshed domain is shown in Fig. 2. Boundary layer meshing strategy was adapted near the hub and casing walls to predict boundary layer and its separation with a higher level of accuracy.

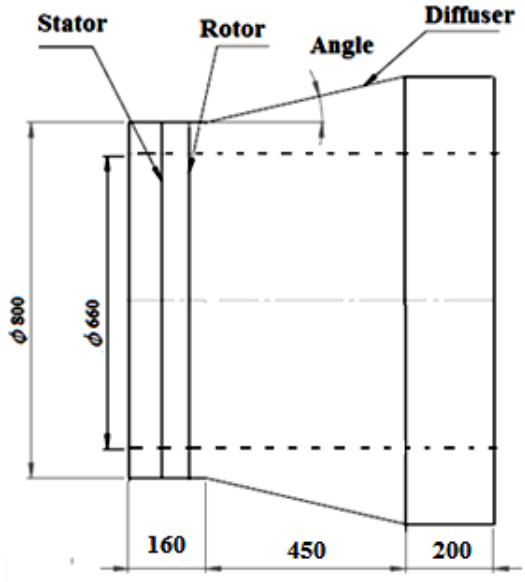

Fig. 1. Schematic representation of Tubine-Diffuser model.

In this case the computational domain has been chosen as a 2-D lamina equivalent to upper half of the mid-sectional view of 3-D computational domain. For this two dimensional computational domain, the left boundary is assigned as inlet, the right edge is taken as outlet, while the upper and bottom bounding edges are assigned with no slip wall boundary condition. Similar to the 3-D computational domain, the inner interfaces representing stator and rotor blade rows are assigned with suitable pressure jumps.

3.1 Boundary Conditions

The boundary conditions imposed in the present simulations are as follows:

Inlet: Inlet boundary condition used in the present simulation is pressure inlet. Total pressure at the entrance of turbine stage is specified as 1.4 bar. Intensity of turbulence is specified as intermediate turbulence i.e. 5% with respect to equivalent flow diameter.

Outlet: Pressure outlet boundary is used at the exit of the diffuser where the pressure value reached to atmospheric pressure.

Stator/Rotor: Fan option specified to give boundary conditions in zero thickness discs of computational domain.

Outer covering/Shaft: Wall boundary with no-slip conditions is employed.

The other fluid properties considered in the current computational study are tabulated in Table 1.

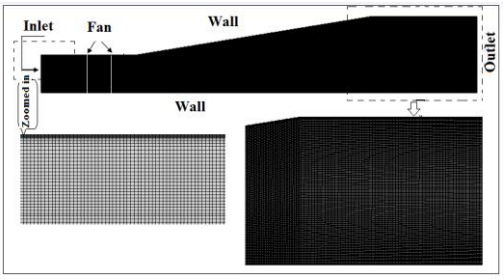

Fig. 2. Tubine-Diffuser domain marked with boundary conditions.

Table 1 Thermodynamic properties used in the CFD simulation

At operating pressure of 101325 Pa and reference temperature of 298.15 K	
Density ρ	1.183 kg/m^3
Specific constant C_P	1004.4 J/(kg.K)
Gas constant R	287.1 J/ (kg.K)
Viscosity	1.831*e^{-5} (N.s)/m^2

The computational domain was initialised with the conditions at the pressure inlet. Further, time marching of the solution was carried out by explicit method. A maximum CFL number of 0.5 was considered for the reasons of stability of the solution. Iterations were continued till the solution reach to steady state. The residuals of mass, energy, momentum and turbulent parameters were set to be 1×10^{-6} as the convergence criteria.

4. Results And Discussion

4.1 Implementation of Actuator Disc Model

In the turbine diffuser computational model, the stator and rotor blades are compressed into zero thickness discs at the location of trailing edge of the blade rows. The flow behaviour across the disc can take a discontinuous jump in order to capture the flow turning and entropy generation developed in the turbine blade row. The behaviour of the calculation domain of an actuator disc in the numerical analysis as shown in Fig.3 has been reported in the work of Liu and Hynes (2002).

The upstream side of the disc represents the inlet of the turbine blade row and the downstream side the outlet of the blade row. In order to implement the actuator disc theory in the turbine stage 'Fan' boundary type was used. Those specified numerical

boundary is considered to be infinitely thin and the pressure drop across the disc is mentioned as the function of the fluid velocity normal to the blade rows. The implementation details of actuator discs are shown in Table 2 based on the following assumptions.

1. Infinitely thin disc area used instead of turbine blade rows and it cannot offer any resistance to air flowing through it.
2. Over the disc, velocity components are uniform.

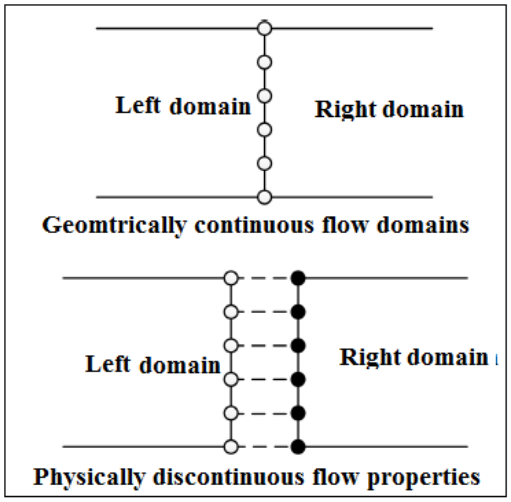

Fig. 3. Sketch of actuator disc model by Liu and Hynes (2002).

Table 2 Boundary conditions

Actuator disc boundary conditions	
Boundary Type	Fan
Pressure Jump Specification	Calculate pressure drop from average conditions
Pressure drop (Pa)	Constant : for Stator 6765.33 for Rotor 16192.57

The pressure drop across the discs due to energy extraction in the turbine blades calculated from the reported turbine stage specifications are as shown in Table 3.

Table 3 Parameters employed in the current simulation under operating pressure 101325 Pa

Specification for Turbine Stage	
Hub/Tip ratio	0.825
Flow coefficient (φ)	0.56
Loading coefficient (ψ)	2.26
Rotor Speed	2700 rpm
Total Temperature	328 K
Total to total pressure ratio	1.3
Turbine total inlet pressure	1.4 bar

4.2 Grid Independency Study

Grid independency study has also been carried out to ensure elimination of grid resulted error in the solution, by changing the node values at the edges of the computational domain. The solution becomes more and more accurate with refinement of mesh. To analyze the grid independency of numerical solution, the surface pressure values obtained for three levels of grids are compared in Fig. 4. Here the coarser mesh had 200000 cells, whereas the medium and fine grids contained 242000 and 288000 cells, respectively. Fig. 3 clearly shows that there is no significant difference in the results obtained on medium and fine grid levels. Hence a moderate mesh having 242000 quadrilateral cells is found to be sufficient enough for the accurate simulation of flow field of interest.

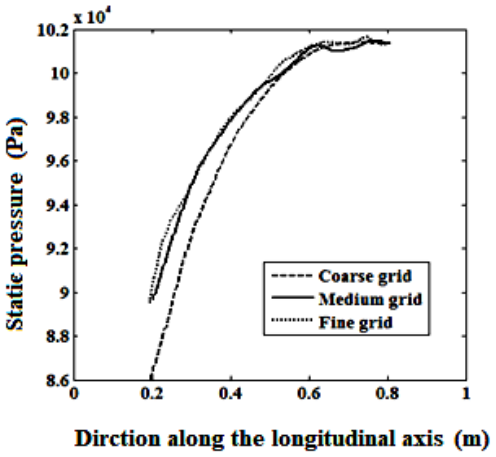

Fig. 4. Comparison of static pressure distribution along the diffuser section of model.

4.3 Validation of Numerical Results

The first objective of the current research is the validation 2-D axisymmetric actuator disc model by comparing its predictions with reported experimental measurements of Behr (2007).

To validate the current numerical frame work, the same geometrical features of turbine and flow conditions of experiment Behr (2007) were followed in the numerical simulation. The details of specifications employed for the experiments, which were again used for the establishment of numerical simulation setup for the current simulations are summarized in Table 3. The simulations have been performed till the solutions converged to a steady state.

Finally, the steady state results are used to validate the accuracy of the current simulation strategy. The numerically obtained Mach number distribution along the radial direction at the exit of the stator is compared with corresponding experimental data in Fig. 5. It can be noticed that they are in close agreement.

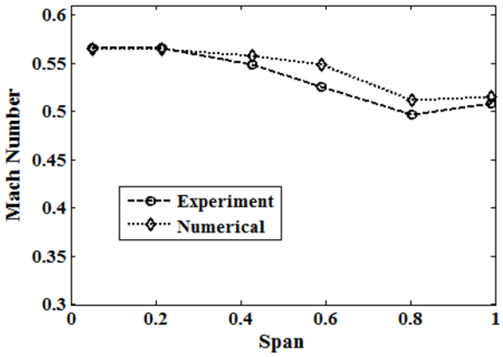

Fig. 5. Comparison of Mach number distribution at the stator exit.

Further, the total to total isentropic efficiency of turbine stage at the design operating point is calculated as 91% using Equation (3).

$$\eta_{tt} = \frac{\Delta h}{\Delta h_{is}} = \frac{Power / \dot{m}}{C_p T_{t,in}\left[1 - \left(\frac{P_{t,out}}{P_{t,in}}\right)^{\frac{\gamma-1}{\gamma}}\right]} \quad (3)$$

The values of isentropic efficiency of the turbine stage derived from the present numerical solution and that obtained from the experimental results are compared in Fig.6. Again these data are also in good agreement. The closely matching results in figures 5 and 6 prove the accuracy of the current actuator disk model in predicting the overall flow field behind the stator and rotor. Hence, further studies were carried out using this simplified model to investigate the effect of diffuser angle on the performance of turbine stage.

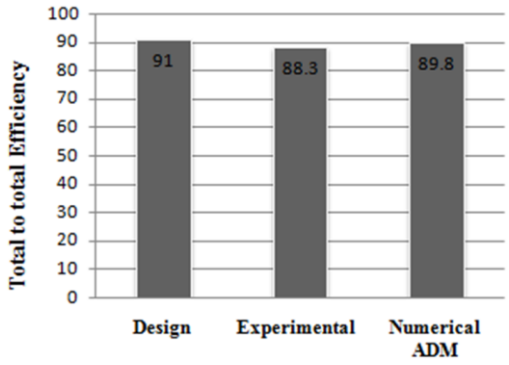

Fig. 6. Comparison of Isentropic total to total efficiency.

4.4 Effect of Divergence Angle on the Performance of Gas Turbine Stage

In the previous section, it is shown that 2D axisymmetric numerical results obtained with actuator disc model are in good agreement with actual experimental results, thus proved the applicability of present computational frame work for turbine diffuser section simulation. It is also observed that the employed actuator disc concept offers a great advantage in terms of reduced computational effort, as it eliminates modelling of flow through stator blades and moving blade rows. Moreover, this model does not require mesh rotation or mesh adjustment, which in turn increases saving of computational time in terms of excluded node and face re-computing. Hence, after verifying the validity of 2D axisymmetric actuator disk model, the focus of the present investigation got shifted to exploration of effect of diffuser angle on the performance of gas turbine stage.

In this study, four different divergence angles were tested. The investigated divergence angles include 7^0, 9^0, 11^0 and 13^0. The variation in divergence was realized by keeping the inlet radius and the total length of the diffuser as constant. The computational domains for all four divergence angle cases were modeled and meshed by following the same strategy employed in the grid independency study. In addition to that, the solution strategy was also kept the same. Thus obtained steady state results are then employed here to explore the effect of divergence angle on the performance of gas turbine stage.

The Mach contours of four different diffuser angle cases are compared in Figs. 7-10. The streamlines are also overlapped on the contours to clearly demonstrate the flow features. It can be seen from Fig. 7 that there is a flow acceleration across the stator and rotor sections. The rise in velocity across the stator is due to energy conversion. In other words, the static pressure drop occurred in the (see Fig. 11) stator is the reason for the rise in Mach number across the stator. However, the Mach number at the outlet can be seen to be lesser in comparison with that of rotor inlet. This flow deceleration is also associated with a drop in pressure. This is due to the energy transfer in the rotor in the form of work. The flow behind the rotor then enters the diffuser section where it gets decelerated further. Here the subsonic flow deceleration across the diffuser section raises the static pressure continuously as shown in Fig 11. That means the flow in the diffuser happens against an adverse pressure gradient, a higher value of which may end up in a separation of the flow. The Mach contours and overlapped streamlines are not showing any flow separation for low divergence angles of 7^0 and 9^0. Whereas, in the case of diffuser section with divergence angle of 11^0, separated nature of the flow at the diffuser outer wall is clearly visible. Further increase of divergence angle to 13^0 resulted in flow separations both at outer and inner walls of the diffuser section. Two different recirculation regions observed in Fig. 10 are due to such separations of the flow.

The pressure variations along the outer walls of different stage configurations are further compared in Fig. 11 to understand the effect of divergence angle on the turbine exit pressure. This comparison shows that the minimum value of turbine exit pressure occurs in the case of diffuser having 9^0 divergence angle. Moreover, the turbine exit value is observed to be decreasing with initial increase in divergence angle till 9^0, further increase in diffuser

angle increases the turbine exit pressure and even affects the upstream section of the turbine rotor. These adverse effects are more pronounced in the case of diffuser with the highest divergence angle (13^0). The lower the value of turbine exit pressure for a given turbine inlet pressure the higher would be the power output. Hence, in this connection turbine stage equipped with a diffuser of 9^0 divergence angle can be observed as the most promising one in terms of improved power output.

In addition, the pressure coefficient variation along the hub and casing of turbine diffuser with different casing angles are also compared in Figs. 12 (a-d). Very sharp expansion near the diffuser inlet is the reason for the very low vales of pressure coefficient on the casing surface. Further, these comparisons also evidence the suitability of diffuser with 9^0 divergence angle.

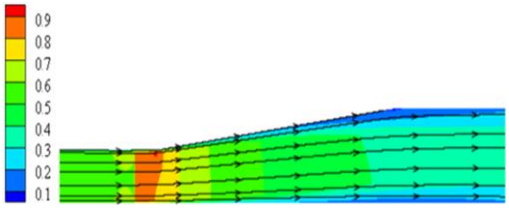

Fig. 7. Stream traces shown over Mach contours for 7 degree diffuser angle.

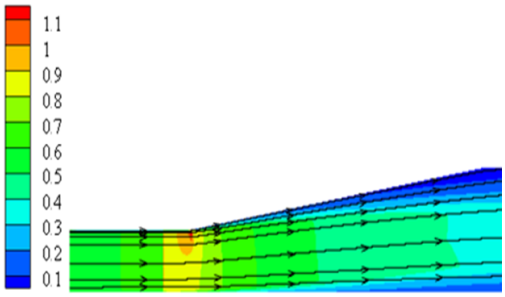

Fig. 8. Stream traces shown over Mach contours for 9 degree diffuser angle.

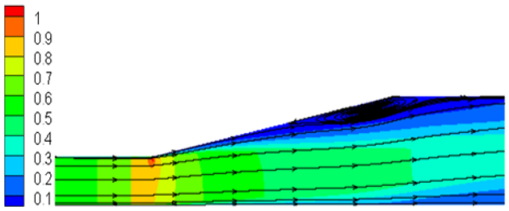

Fig. 9. Stream traces shown over Mach contours for 11 degree diffuser angle.

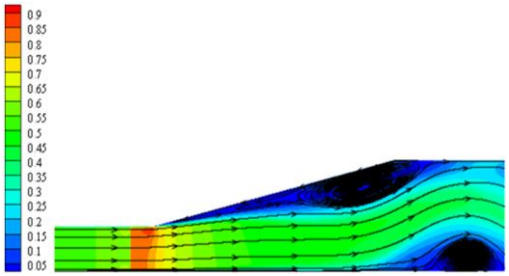

Fig. 10. Stream traces shown over Mach contours for 13 degree diffuser angle.

Although pressure comparisons fall light on the suitability of a given divergence angle on the basis of turbine exit pressure, that information is not enough to propose a given diffuser as the best one. Additionally one has to look into the chance of occurrence of flow separations while using a diffuser section. It is not just the static pressure that decides the performance; in addition, the total pressure recovery is also important.

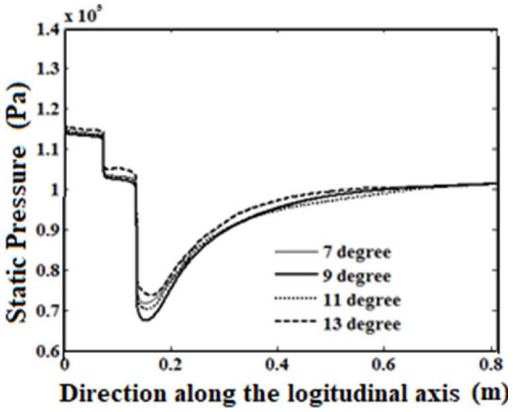

Fig. 11. Comparison of static pressure distribution along the turbine - diffuser.

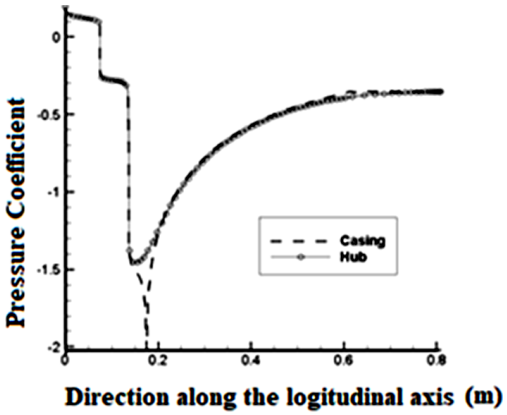

Fig. 12(a). Pressure coefficient variation along the hub and casing at 7 degree diffuser angle.

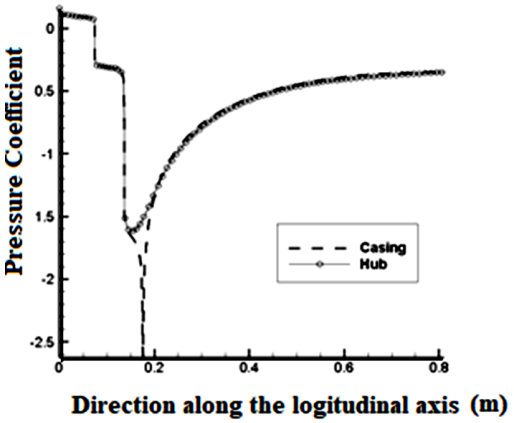

Fig. 12(b). Pressure coefficient variation along the hub and casing at 9 degree diffuser angle.

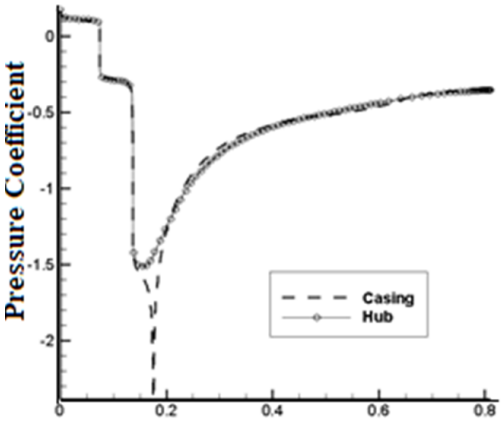

Fig. 12(c). Pressure coefficient variation along the hub and casing at 11 degree diffuser angle.

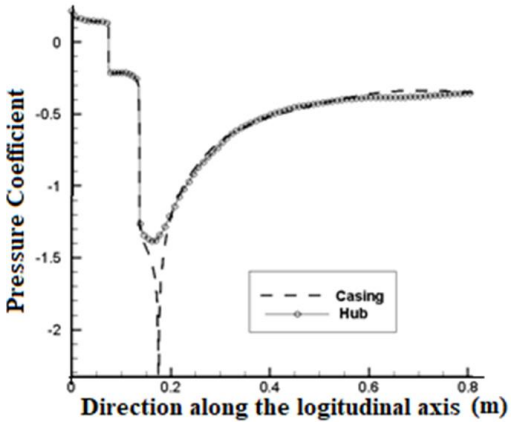

Fig. 12(d). Pressure coefficient variation along the hub and casing at 13 degree diffuser angle.

Generally separation of the flow reduces the total pressure recovery and induces unsteadiness to the system. Hence, to understand the intensity and extension of flow separation generated by different diffuser sections, the axial velocity variations along the radial direction from the hub to casing at an axial location of z = 50 cm downstream of the domain inlet are compared in Fig. 13. This axial location has purposefully chosen for the analysis by considering the fact that the core of the largest separation zone near the casing was observed for the diffuser of 13^0 divergence angle at this location. It can be seen from the Fig. 13(a) that the axial velocity values are negative near the casing for the diffusers of higher divergence angles (11^0 and 13^0). However, for 7^0 and 9^0 cases, there are no negative values of axial velocity in the velocity profiles, which prove existence of an attached nature of flow in those cases.

Further, to understand the effect of separation on the total pressure recovery, the total pressure distributions are also compared at the same reference location mentioned in the previous discussion. It is very clear from Fig. 13(b) that the average value of total pressure in the reference plane is very high for both 7^0 and 9^0 cases. Although the total pressure values are seen to be a little bit high at the mid sections of the diffusers of higher divergence angles, the total pressure values significantly dropped near the hub and casing sections due to the separation of the flow. These reference frame comparisons clearly show that an increase in divergence angle beyond an optimum value will enhance the total pressure loss.

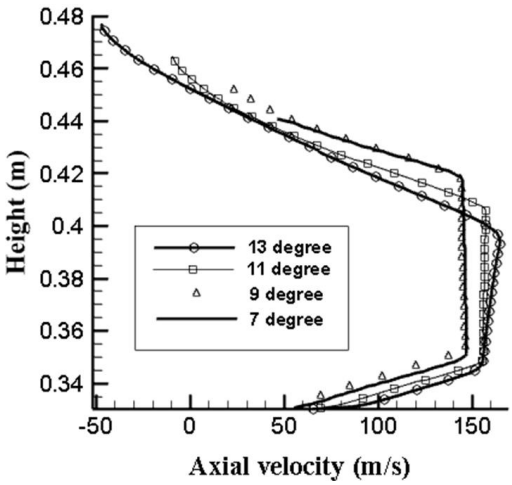

Fig. 13 (a) Axial velocity variations along the radial direction from the hub to casing at an axial location of z =50 cm.

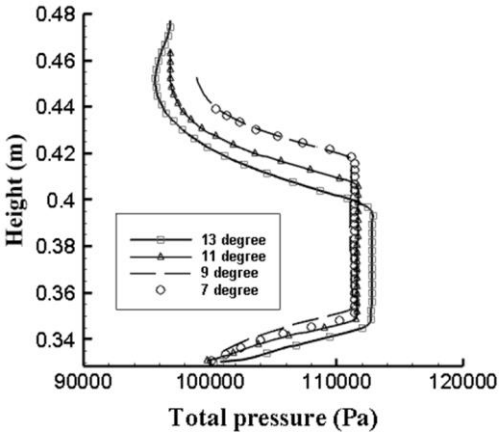

Fig. 13(b). Total pressure variations along the radial direction from the hub to casing at an axial location of z =50 cm.

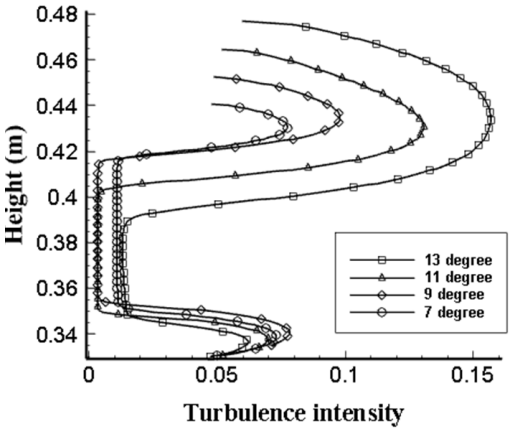

Fig. 13(c). Turbulence intensity variations along the radial direction from the hub to casing at an axial location of z =50 cm.

Finally, the effects of divergence angle on the turbulent characteristics of the flow are also studied. The turbulent intensity comparisons made on a radial plane considered at the reference axial location evidence the increased nature of turbulent intensity within the separation zone. The turbulent intensity values are observed to be minimal at the clean flow region. However, the same are found to be higher near the walls of hub and casing for all the diffuser geometries. Moreover, the distribution is very symmetric in case of 7^0 diffuser. The turbulent intensity values are noticed to be increasing rapidly as the divergence angle increases. The parabolic nature of the turbulent intensity curves near the hub and casing are due to boundary layer developing over those surfaces. Larger values of turbulent intensity can be noted from Fig.13(c). Such elevated turbulent intensities are the results of momentum transfer caused due to stagnant vortices in the separated region.

5. CONCLUSION

The present study shows that the actuator disc model is capable of predicting the performance of gas turbine diffusers accurately with less computational effort. Another major revelation of this work is that a 2D axisymmetric actuator disk flow model is good enough in simulating the flow behavior in a gas turbine diffuser with reasonable accuracy. From the current study it is clearly seen that when the divergence angle of the diffuser is increased, the pressure recovery capacity increased due to the higher rate of diffusion but losses due to pressure recovery increases, as result the flow separation follows a growing trend. The turbine stage equipped with a diffuser of 9^0 divergence angle is observed as the most promising one in terms of improved power output. Increase in divergence angle of the diffuser is observed to be advantageous as far as shorter diffuser design is concerned. However, selection of very high divergence angle is noticed to be resulting in separation of the flow field.

REFERENCES

Ackert J, (1967). Aspect of Internal Flow. Fluid Mechanics of Internal Flow.

Behr, T. (2007). *Control of rotor tip leakage and secondary flow by casing air injection in unshrouded axial turbines* (Doctoral dissertation, ETH Zurich).

Desideri, U. and G. Manfrida (1995, June). Flow and turbulence survey for a model of gas turbine exhaust diffuser. In *ASME 1995 International Gas Turbine and Aeroengine Congress and Exposition* (pp. V003T06A030-V003T06A030). American Society of Mechanical Engineers.

Djebedjian, B. and J. P. Renaudeaux (1998). Numerical and experimental investigation of the flow in annular diffuser. In *ASME Paper FEDSM98–4967*, June. presented at the 1998 ASME Fluids Engineering Division Summer Meeting, Washington, DC.

Fleischer, F., C. Koerner and J. Mann (1989). Flow guiding and distributing devices on the exhaust side of stationary gas turbines. In *ASME 1989 International Gas Turbine and Aeroengine Congress and Exposition* (pp. V004T09A018-V004T09A018). American Society of Mechanical Engineers.

Foote, T. and R. Agarwal (2012, July). Optimization of power generation from shrouded wind turbines. In *ASME 2012 6th International Conference on Energy Sustainability collocated with the ASME 2012 10th International Conference on Fuel Cell Science, Engineering and Technology* (pp. 1325-1331). American Society of Mechanical Engineers.

Froude, R. E. (1889). On the part played in propulsion by differences of fluid pressure. *Trans. Inst. Naval Architects*, 30, 390.

Hawthorne, W. R. and J. H. Horlock (1962). Actuator disc theory of the incompressible flow in axial compressors. *Proceedings of the institution of Mechanical Engineers* 176(1), 789-814.

Liu, J. J. and T. P. Hynes (2002, January). The Investigation of Turbine and Exhaust Interactions in Asymmetric Flows: Part 2—Turbine-Diffuser-Collector Interactions. In *ASME Turbo Expo 2002: Power for Land, Sea, and Air* (pp. 179-188). American Society of Mechanical Engineers.

Mikkelsen, R. (2003). *Actuator disc methods applied to wind turbines*. Technical University of Denmark.

Rankine, W. J. M. (1865). On the Principles of the Action of Propellers. *Trans. Inst. Nav. Arch*. 6, 13.

Réthoré, P. E., N. N. Sørensen, F. Zahle and J. Johansen (2008). Comparison of an actuator disc model with a full rotor cfd model under uniform and shear inflow condition. In *Book of abstracts; 4th PhD seminar on wind energy in Europe*, Magdeburg (pp. 123-126).

Horlock, J. H. (1978). *Actuator disk theory-Discontinuities in thermo-fluid dynamics*. New York, McGraw-Hill International Book Co., 1978. 256 p.

Venugopal M, Somashekar (2015), Design and Analysis of Annular Exhaust Diffuser for Jet Engine. International *Journal of Innovative Research in Science, Engineering and Technology* 4(7).